

GSRM: Building Roadmaps for Query-Efficient and Near-Optimal Path Planning Using a Reaction Diffusion System

Christian Henkel¹, Marc Toussaint², and Wolfgang Hönig²

Abstract—Mobile robots frequently navigate on roadmaps, i.e., graphs where edges represent safe motions, in applications such as healthcare, hospitality, and warehouse automation. Often the environment is quasi-static, i.e., it is sufficient to construct a roadmap once and then use it for any future planning queries. Roadmaps are typically used with graph search algorithm to find feasible paths for the robots. Therefore, the roadmap should be well-connected, and graph searches should produce near-optimal solutions with short solution paths while simultaneously be computationally efficient to execute queries quickly.

We propose a new method to construct roadmaps based on the Gray-Scott reaction diffusion system and Delaunay triangulation. Our approach, GSRM, produces roadmaps with evenly distributed vertices and edges that are well-connected even in environments with challenging narrow passages. Empirically, we compare to classical roadmaps generated by 8-connected grids, probabilistic roadmaps (PRM, SPARS2), and optimized roadmap graphs (ORM). Our results show that GSRM consistently produces superior roadmaps that are well-connected, have high query efficiency, and result in short solution paths.

I. INTRODUCTION

To use path finding algorithms such as A* for robot motion planning, a discretization of the environment is necessary. A common approach is to discretize the environment as a grid. However, such gridmaps generalize to non-rectangular environments ineffectively. More generally, an environment can be discretized to a roadmap, which is a graph where vertices are locations that the robot can occupy, and the edges are possible motions between these locations. A simple graph search in this roadmap will result in a feasible motion through the given environment. The quality of the path is measured by its length and directly determined by the construction of the roadmap, assuming an optimal graph search algorithm.

The construction of a roadmap has multiple goals. First, the roadmap should be well-connected, such that any two vertices are connected by a path. Second, the roadmap should allow for efficient queries, i.e. it should have few vertices, because this improves the planning time when searching for a path. Third, the roadmap should allow for short paths between any two vertices. Finally, it is desirable to compute or update roadmaps efficiently. Our work focuses mostly on

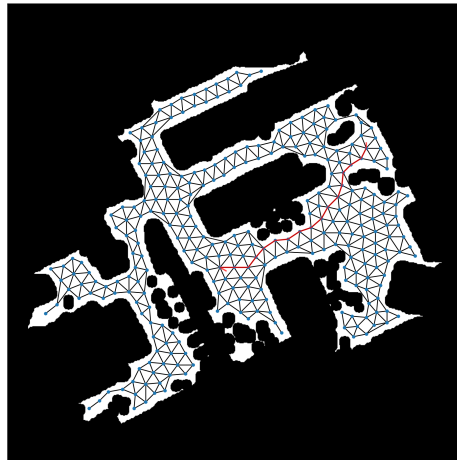


Fig. 1. Example roadmap with 290 nodes and 957 edges on the map *Slam* from Fig. 3d. Blue dots are the vertices of the roadmap, black lines are the edges. The red line is an example path with a length of 0.479. The roadmap was produced from the simulation of the Gray-Scott system shown in Fig. 2d.

the path length while maintaining connectedness and query-efficiency. The roadmap it built once and then used for any path finding query. Therefore, the query-efficiency and path length of the roadmap are more important properties than the computational efficiency of its construction. While generally, roadmaps are often constructed in high-dimensional spaces, e.g., for manipulators, we focus this paper and the evaluation explicitly on the two-dimensional case that is common for mobile robots.

A reaction diffusion system is a class of partial differential equations that model the diffusion of substances and their reaction with each other. This model can produce spotted patterns [1] that fill a given space, see Fig. 2d. It can be seen that these spots have a similar density throughout the accessible space. This allows the generation of a roadmap graph by using the center points of these spots as vertices and connecting them locally by edges. To find the edges, we use the Delaunay triangulation [2]. The resulting roadmap is depicted in Fig. 1. We call this approach Gray-Scott Model Based Roadmap (GSRM).

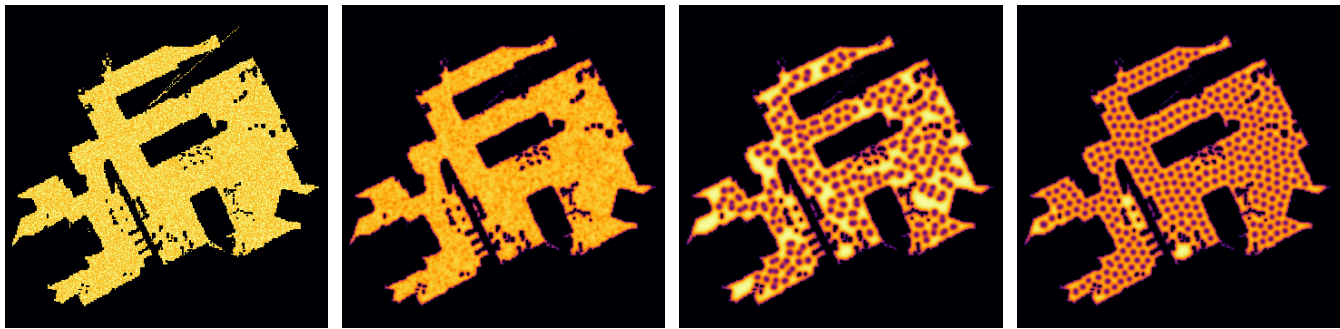
II. RELATED WORK

The basic idea of Probabilistic Roadmaps (PRMs) is to sample random points from the given configuration space and

¹Robert Bosch GmbH, Stuttgart, Germany hec21e@bosch.com

²TU Berlin, Germany {toussaint, hoenig}@tu-berlin.de

The research was partially funded by the Deutsche Forschungsgemeinschaft (DFG, German Research Foundation) - 448549715.



(a) At the beginning of optimization after random initialization. (b) After 10 simulation steps. (c) After 500 simulation steps. (d) After 10000 simulation steps.

Fig. 2. Concentration of substance U over time. The grid size is $l = 300$. Black areas are obstacles, where the concentration is zero. The brighter the color, the higher the concentration of substance U . It is visible how the spotted pattern emerges.

connect these with motions generated by a local planner [3]. These roadmaps are constructed once and can then be queried multiple times at runtime. These queries can be performed with a classic graph search like A* [4] to retrieve viable motions through the given configuration space. A review over different PRMs is given in [5].

One version that is asymptotically optimal is called PRM* [6]. Here, vertices are connected to more vertices compared to the traditional PRM, to ensure asymptotical optimality. As a drawback this makes maps denser, which leads to more expensive path finding queries. Since it is not delivering sparse roadmaps, we do not evaluate against it.

The alternative approach called SParse Roadmap Spanner (SPARS) maintains near-optimality, but it additionally enforces the sparsity of the roadmap [7]. It consists of one dense asymptotically optimal roadmap, similar to PRM* and an additional spanner of that graph that maintains sparsity by only adding new points if necessary for path quality or connectivity. SPARS2 is an extension that improves the computational performance of the roadmap construction [8]. We evaluate our approach against SPARS2, because we consider it to be the state of the art in terms of sparsity and path length. We will show that our roadmap produces shorter paths with the same number of vertices.

Another work constructs a roadmap by focussing only on critical sections, e.g. doorways [9]. This can also lead to a sparse graph. However, we want to construct a graph that spans the whole configuration space because we want to use it for the full path of the robot.

Roadmaps can also be built tailored to specific queries. Rapidly-exploring Random Tree (RRT), introduced by LaValle [10], involves the incremental growth of a tree-like structure from an initial pose. This growth is achieved by systematically sampling potential new poses and verifying their connectivity within the environment. In our research, we place particular emphasis on the multi-query approach to motion planning instead. Rather than constructing a new roadmap for each navigation task, we aim to leverage a roadmap that has been pre-computed and encodes informa-

tion about the environment.

It is also common to construct roadmaps using Voronoi graphs [11]. For example, [12] proposes a method to build a roadmap by using so-called local clearance triangulations. This method can be used to generate paths with an arbitrary clearance. There are also approaches to generate generalized Voronoi diagrams for sensor coverage [13]. A method that uses Hamilton-Jacobi Skeletons for dynamic topological SLAM maps is [14]. A similar approach can also be used to generate navigation roadmaps for robot exploration [15]. SphereMap [16] builds a roadmap for UAV exploration in subterranean environments by sampling spherical segments. A roadmap for exploration of mobile robots can be built by sampling disks and connecting them with a visibility graph [17]. We do not consider these methods in our evaluation, because they are optimized for area coverage of a sensor or for exploration, not for path planning.

Roadmaps can also be specifically constructed for multiple agents. For example, by optimization [18] or hierarchical segmentation [19]. In [20], SPARS is used to plan trajectories for heterogeneous swarms of different aerial and ground robots. Optimized Roadmap Graph (ORM), presented in [18] initializes the roadmap poses randomly and optimizes them by minimizing the length of randomly sampled paths. We evaluate GSRM against it in the evaluation section. While generally, the multi-agent use case can also be solved by the roadmaps we propose, it is not the focus of this paper.

Reaction diffusion systems are a class of partial differential equations that model the diffusion of substances and their reaction with each other. They can show complex patterns, also called *Turing Patterns* [21]. One of the most famous examples is the Gray-Scott system [22]. When simulated in a grid, it produces spotted patterns [1] as can be seen in Fig. 2.

Reaction diffusion systems have been used in robotics before, for example in robot navigation [23]–[26], controller synthesis [27], exploration [28], and sensor coverage [29].

III. PROBLEM FORMULATION

Let $\mathcal{C}_{\text{free}} \subset \mathbb{R}^2$ be the free space of the environment. Let $\mathcal{V} \subset \mathcal{C}_{\text{free}}$ be the vertices of the roadmap. And let $\mathcal{E} \subseteq \mathcal{V} \times \mathcal{V}$ be the edges of the roadmap. This forms the roadmap $\mathcal{G} = \langle \mathcal{V}, \mathcal{E} \rangle$.

We assume planning queries to be defined by a start location $s \in \mathcal{C}_{\text{free}}$ and a goal location $g \in \mathcal{C}_{\text{free}}$. In $\mathcal{C}_{\text{free}}$, we define the continuous path $\pi_c^{\text{sg}} : \mathbb{R} \rightarrow \mathcal{C}_{\text{free}}$ from s to g . We use the vertices closest to s and g as start vertex v_s and goal vertex v_g , respectively, i.e.

$$\begin{aligned} v_s &= \arg \min_{v \in \mathcal{V}} \|v - s\| \\ v_g &= \arg \min_{v \in \mathcal{V}} \|v - g\|, \end{aligned} \quad (1)$$

where $\|\cdot\|$ is the Euclidean distance.

The discrete path $\pi_d^{\text{sg}} : \{0, 1, \dots, n\} \rightarrow \mathcal{V}$ is defined by $\pi_d^{\text{sg}}(0) = v_s$ and $\pi_d^{\text{sg}}(n) = v_g$, where

$$\forall i \in \{0, 1, \dots, n-1\}, \langle \pi_d^{\text{sg}}(i), \pi_d^{\text{sg}}(i+1) \rangle \in \mathcal{E}. \quad (2)$$

Its length is defined as

$$\text{length}(\pi_d^{\text{sg}}) := \sum_{i=0}^{n-1} \|\pi_d^{\text{sg}}(i+1) - \pi_d^{\text{sg}}(i)\|. \quad (3)$$

Let Π_d^{sg} be the set of all discrete paths from v_s to v_g . Then the shortest path between v_s and v_g is defined as

$$\hat{\pi}_d^{\text{sg}} = \arg \min_{\pi_d^{\text{sg}} \in \Pi_d^{\text{sg}}} \text{length}(\pi_d^{\text{sg}}). \quad (4)$$

We define the length of the path π_c^{sg} in $\mathcal{C}_{\text{free}}$ as the geometric length of the shortest discrete path which includes the distance from s to the first vertex and the distance from the last vertex to g :

$$\text{length}(\pi_c^{\text{sg}}) := \text{length}(\hat{\pi}_d^{\text{sg}}) + \|\hat{\pi}_d^{\text{sg}}(0) - s\| + \|\hat{\pi}_d^{\text{sg}}(n) - g\|. \quad (5)$$

The goal of the roadmap construction is to find a roadmap \mathcal{G} that minimizes the expected length of the paths while limiting the number of vertices in the graph to a maximum number n_{max} :

$$\arg \min_{\mathcal{G}} \int_{(s,g) \in \mathcal{C}_{\text{free}} \times \mathcal{C}_{\text{free}}} P(s,g) \text{length}(\pi_c^{\text{sg}}) \text{ s.t. } |\mathcal{V}| < n_{\text{max}}. \quad (6)$$

In this paper, we assume $P(s,g)$ to be a uniform distribution over $\mathcal{C}_{\text{free}} \times \mathcal{C}_{\text{free}}$.

IV. GRAY-SCOTT SYSTEM

To generate the roadmap we first need to define vertex positions in free space. For this, we use the Gray-Scott system [22]. The Gray-Scott system is a simplified model of a chemical reaction-diffusion system. It models two chemical substances that react with each other and move by diffusion. The substances are generally called U and V and their chemical reaction is defined as



where $x \rightarrow y$ means that reactants x yield products y .

Additionally, the system models a constant addition of substance U according to the feed rate A as well as a constant removal of V according to the kill rate B . The diffusion of the substances is quantified by the diffusion parameters D_U and D_V respectively.

For a certain configuration of the aforementioned variables A , B , D_U , and D_V , it produces stable spotted patterns that fill a given two-dimensional space [30].

A. Simulation

We simulate this system in a grid of $l \times k$ cells, where $u \in \mathbb{R}^{l \times k}$ and $v \in \mathbb{R}^{l \times k}$ are the concentration of substance U and V , respectively. The *Gray-Scott Model Based Roadmap (GSRM) Construction* in Algorithm 1 describes the simulation of the Gray-Scott system. We will elaborate the algorithm in the following.

Algorithm 1 Gray-Scott Model Based Roadmap (GSRM) Construction

```

1: Input:  $A, B, D_U, D_V, l, k, \mathcal{C}_{\text{free}}, u_l, u_h, v_l, v_h$ 
2: Output:  $\mathcal{V}, \mathcal{E}$ 
3:  $u \leftarrow \text{random\_uniform}(l, k, u_l, u_h)$ 
4:  $v \leftarrow \text{random\_uniform}(l, k, v_l, v_h)$ 
5: for  $[0, N]$  do
6:    $\forall (x, y) \notin \mathcal{C}_{\text{free}} : u(x, y) \leftarrow 0$ 
7:    $\forall (x, y) \notin \mathcal{C}_{\text{free}} : v(x, y) \leftarrow 0$ 
8:    $\frac{\delta u}{\delta t} \leftarrow D_U \Delta u - uv^2 + A(1 - u)$ 
9:    $\frac{\delta v}{\delta t} \leftarrow D_V \Delta v + uv^2 - (A + B)v$ 
10:   $u \leftarrow u + \frac{\delta u}{\delta t}$ 
11:   $v \leftarrow v + \frac{\delta v}{\delta t}$ 
12: end for
13:  $v_{\text{threshold}} \leftarrow \begin{cases} 1 & \text{if } v(x, y) > \frac{\max v}{2} \\ 0 & \text{if } v(x, y) \leq \frac{\max v}{2} \end{cases}$ 
14:  $\text{contours} \leftarrow \text{find\_contours}(v_{\text{threshold}})$ 
15:  $\mathcal{V} \leftarrow \emptyset$ 
16: for  $\text{contour} \in \text{contours}$  do
17:    $\text{center} \leftarrow \text{average}(\text{contour})$ 
18:    $\mathcal{V} \leftarrow \mathcal{V} \cup \{\text{center}\}$ 
19: end for
20:  $\mathcal{V}_{\text{dummy}} \leftarrow \text{make\_vertices\_in\_obstacles}(\mathcal{C}_{\text{free}})$ 
21:  $\mathcal{E} \leftarrow \emptyset$ 
22:  $\text{triangles} \leftarrow \text{delaunay}(\mathcal{V} \cup \mathcal{V}_{\text{dummy}})$ 
23: for  $(a, b, c) \in \text{triangles}$  do
24:   for  $e \in \{(a, b), (b, c), (c, a)\}$  do
25:     if  $\text{free}(e, \mathcal{C}_{\text{free}})$  then
26:        $\mathcal{E} \leftarrow \mathcal{E} \cup \{e\}$ 
27:     end if
28:   end for
29: end for
30: return  $\mathcal{V}, \mathcal{E}$ 

```

Let u_l and u_h be the lower and upper bounds of the concentration of substance U and v_l and v_h be the lower and upper bounds of the concentration of substance V . We initialize u with values between u_l and u_h in line 3 and

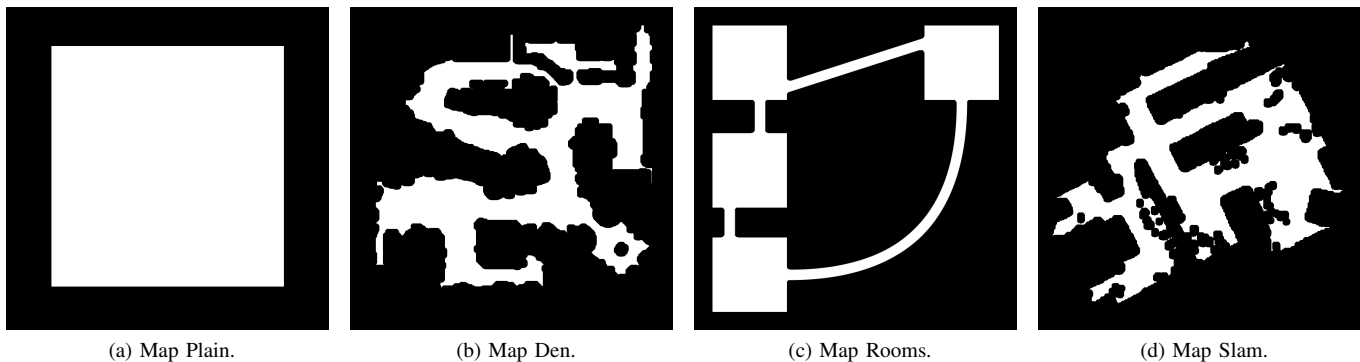


Fig. 3. Maps used in evaluation. Gray and black areas are obstacles. White areas are free space.

v with values between v_l and v_h in line 4. The function `random_uniform(l, k, x, y)` returns an $l \times k$ matrix filled with values, each independently sampled from the uniform distribution of values between x and y .

At the borders of the grid and in obstacles, we set both concentrations to zero in line 6. This stops the pattern from spreading into these regions. In line 8 and line 9, we calculate the update for the concentrations of the substances according to the following differential equations:

$$\begin{aligned} \frac{\delta u}{\delta t} &= D_U \Delta u - uv^2 + A(1 - u) \\ \frac{\delta v}{\delta t} &= D_V \Delta v + uv^2 - (A + B)v, \end{aligned} \quad (8)$$

where Δ is the Laplace operator and all other operations are performed element-wise.

The update is performed in a loop, N times. See Fig. 2 for an example of the concentration of substance U at different states of the simulation.

B. Identifying Vertices

Based on the result of the simulation of the Gray-Scott system, we have to identify the separate spots in Fig. 2d and use them as vertices \mathcal{V} of the roadmap to produce a result as shown in Fig. 1. First, we transform the concentration of substance V into a binary image by thresholding it at half of the maximum concentration in line 13 of Algorithm 1. Then we apply the border following algorithm [31] to separate the spots in line 14. The function `find_contours(x)` is called on the binary image x and returns a list of unique contours, each represented as a list of points. The lists include all the outermost points per contour, i.e. those that have the value 1 and at least one neighbor with the value 0.

Based on the contours, we estimate the center of mass of each spot. We take the average over all points of the contour in line 17. Here, the method `average(contour)` takes the points that are part of the contour of the given spot and return their centroid. The result is a set of points \mathcal{V} that are the vertices of the roadmap.

To avoid artifacts in the following step, we need to additionally create dummy vertices in line 20. These are vertices

that are located in the non-free areas of the environment. If they would not exist, the following Delaunay triangulation would produce a lot of small, acute triangle in the areas close to obstacles. However, these vertices will not be considered in the final roadmap.

C. Identifying Edges

The next step is to identify the edges \mathcal{E} of the roadmap. We use the Delaunay triangulation [2] for this purpose. The result is a set of triangles calculated in line 22 of Algorithm 1. In lines 23 to 29 we add an edge between each pair of vertices that are connected by a triangle side iff the edge (a, b) is free, meaning that the straight line between a and b is a subset of $\mathcal{C}_{\text{free}}$:

$$\text{free}((a, b), \mathcal{C}_{\text{free}}) = (tb + (1 - t)a) \in \mathcal{C}_{\text{free}}, \forall t \in [0, 1]. \quad (9)$$

V. EVALUATION

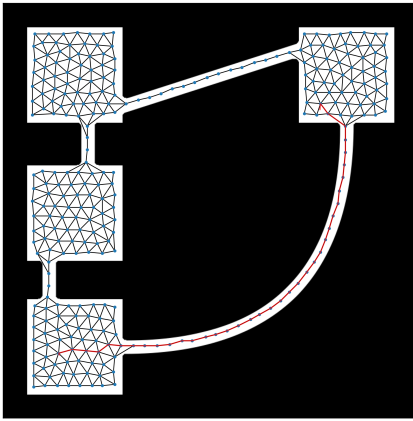
The Gray-Scott Model Based Roadmap (GSRM) algorithm is implemented in C++ using methods from the *OpenCV* library¹. The source code is publicly available².

For the evaluation we rely on four maps with different properties, that are all located in the unit square $[0, 1]^2$:

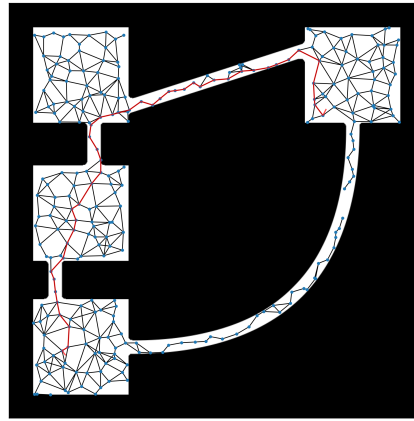
- **Map Plain** in Fig. 3a is an open square with no obstacles. This map demonstrates how the roadmaps allow the agents to move in an open space.
- **Map Den** in Fig. 3b is from a path-finding benchmark [32]. Its special property is that it has comparatively organic shapes and we use it to evaluate the performance of the roadmaps in a more complex environment.
- **Map Rooms** in Fig. 3c is a map with 4 rooms connected by narrow corridors. One of the corridors is curved and we want to check how and if the roadmaps can connect through it.
- **Map Slam** in Fig. 3d is a map that was achieved by running *SLAM* on a real robot in a household environment. It was included to evaluate the performance of the roadmaps in a real-world environment.

¹<https://opencv.org/>

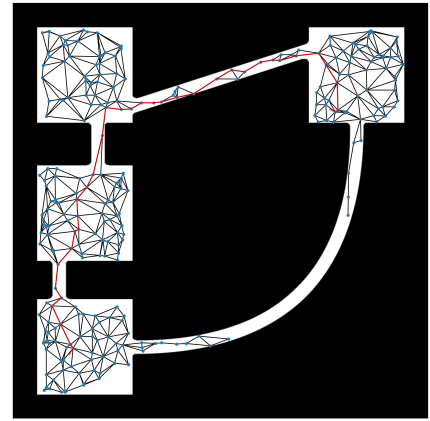
²<https://ct2034.github.io/miriam/iros2024/>



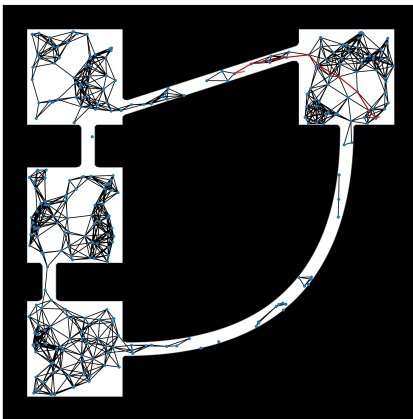
(a) Example of a roadmap with 290 vertices and 963 edges generated by the GSRM algorithm. The path has a length of 1.134, which is the shortest path of all evaluated roadmaps.



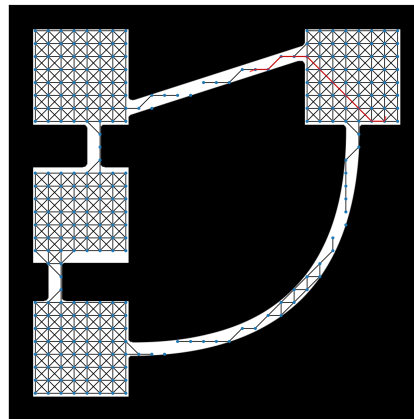
(b) Example of a roadmap with 272 vertices and 520 edges generated by SPARS2. The path has a length of 1.401.



(c) Example of a roadmap with 270 vertices and 932 edges generated by ORM. The path has a length of 1.381.



(d) Example of a roadmap with 282 vertices and 1207 edges generated by PRM. The path has a length of 0.448.



(e) Example of a gridmap with 298 vertices and 877 edges. The path has a length of 0.413.

Fig. 4. Examples of roadmaps generated by different algorithms in map *Rooms*. The red line is an example path. The paths for GSRM, SPARS2, and ORM share the same start and goal points, while the paths for PRM and Gridmap also share the same start and goal points. The last two examples use a different path query, because the query from the first examples are not successfully computable with them.

TABLE I
PARAMETERS FOR THE GSRM ALGORITHM.

Parameter	N	D_U	D_V	A	B	u_l	u_h	v_l	v_h
Value	10 000	0.14	0.06	0.035	0.065	0.8	1.0	0.0	0.2

We compare the GSRM algorithm with the following algorithms:

- **SParse Roadmap Spanner 2 (SPARS2)** [8]. Fig. 4b shows an example of a roadmap generated by SPARS2. Note that we did not find hyperparameters for SPARS2 to generate roadmaps with as small number of vertices as we achieved with the other algorithms.
- **Optimized Roadmap Graph (ORM)**, a variant of [18] where all edges are undirected. Fig. 4c shows an example of a roadmap generated by ORM.
- **Probabilistic Roadmap (PRM)** [3]. Fig. 4d shows an example of a roadmap generated by PRM. We used an implementation where vertices are connected if they are within a distance δ of each other. We set δ such that the number of edges is the same as for GSRM.
- **Gridmap**, an 8-connected gridmap that has all vertices and edges removed that are in obstacles. Fig. 4e shows an example of a gridmap.

For all algorithms, we have chosen sets of parameters such that the number of vertices is similar across the algorithms. In

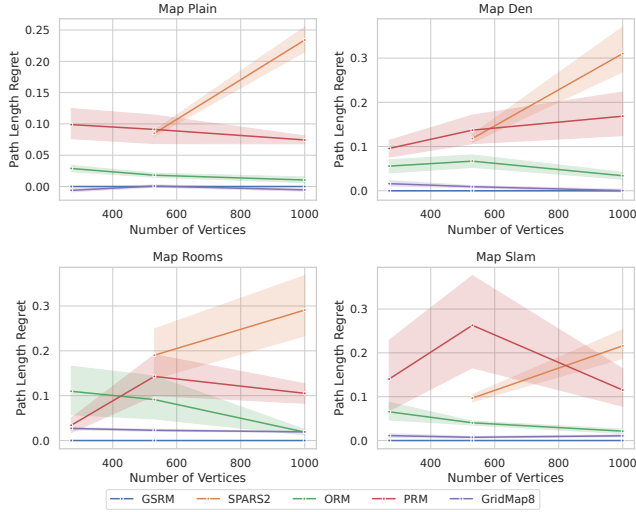


Fig. 5. Average path length regret of the shortest path between two random points in C_{free} for different roadmap types. The shaded areas show the standard deviation across 100 trials. GSRM provides the shortest paths in maps other than *Plain*.

the GSRM algorithm, we can control the number of vertices by changing the resolution $l = k$. For the other parameters, see Table I. These values are necessary to produce a robust spotted pattern in the simulation.

For the evaluation, we approximate the distribution in (6) numerically by a 100 discrete pairs of points per configuration.

A. Path length

We evaluate the quality of the roadmap by measuring the path length of the shortest path between two random points in C_{free} . For all roadmap configurations 10 roadmaps were built. All roadmaps are evaluated with the same 100 pairs of points. The path length is evaluated according to (5). To find the shortest path in the roadmap graph, we use the A^* algorithm [4] from the *Boost* library³ with the Euclidean distance as heuristic.

Fig. 5 shows the average path length regret of the shortest path between two random points in C_{free} for different roadmap types on different maps. The regret per datapoint is calculated by

$$\text{regret} = (\text{pl}_{\text{other}} - \text{pl}_{\text{GSRM}}) / \text{pl}_{\text{other}},$$

where pl_{other} refers to the path length produced on the respective other roadmap, while pl_{GSRM} refers to the one on our roadmap.

It shows that the GSRM algorithm generates roadmaps with a lower path length than the other algorithms in all maps except *Plain*. In the map *Plain*, the 8-connected gridmap produces shorter paths, because it is denser in terms of edges per vertex. Maps that are more structured, such as *Den* and *Rooms*, show a larger difference in path length between the

³<https://www.boost.org>

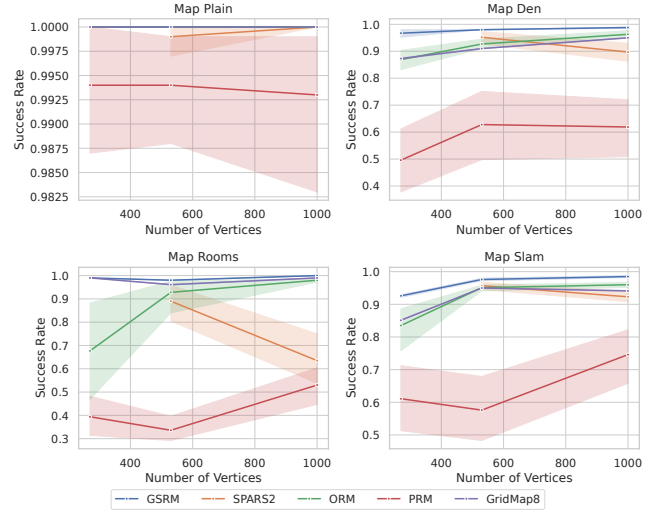


Fig. 6. Success rate of the different algorithms for the path planning. A success rate of 1.0 means that all 100 paths were successful. It is visible that the GSRM algorithm has the highest success rate in all maps.

GSRM algorithm and the other algorithms. This is because the GSRM algorithm can generate roadmaps that adapt to the structure of the environment, while especially the 8-connected gridmap is not able to do so. Generally, for most roadmaps, the path length regret decreases with the number of vertices. The benefit of the GSRM algorithm is that it can generate roadmaps with a low path length even with a low number of vertices.

For the roadmaps PRM and SPARS2 it is visible that the regret increases with a higher number of vertices. This is counterintuitive because it is generally expected that higher numbers of vertices lead to shorter paths. But it can be explained by taking the success rates into account: If less path queries are successful, those that are still successful may result in longer paths.

B. Success Rate

We evaluate the success rate of the roadmap by measuring the fraction of successful path planning queries. As discussed before, paths are planned between two random points in C_{free} . A path then includes the section from the start point to the first vertex and from the last vertex to the goal point. We consider a path unsuccessful if there is no path connecting the two vertices in the roadmap or if there is no free path on the line between the start point and the first vertex or the last vertex and the goal point. This was also evaluated for the 100 same pairs of start and goal configurations per roadmap on 10 roadmaps per configuration.

Fig. 6 shows the success rate of the different algorithms for the path planning. The GSRM algorithm has the highest success rate in all maps. This can be the fact that other roadmaps have a high likelihood of being disconnected on more structured maps. It is visible that for most roadmaps, the success rate increases with the number of vertices. The

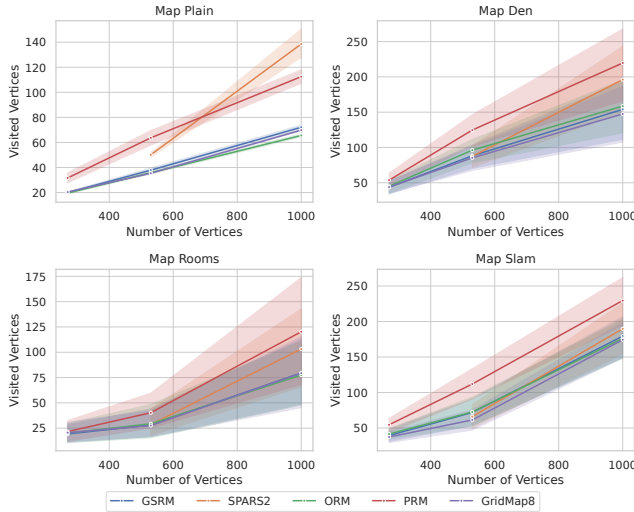


Fig. 7. Average number of visited vertices in A* path planning for different roadmap types. The shaded areas show the standard deviation. GSRM has a comparable number or smallest number of visited vertices.

benefit of the GSRM algorithm is that it can generate roadmaps with a high success rate even with a low number of vertices.

Also for the GSRM roadmap, the success rate is not always 1.0. For example on the map *Slam* with the lowest number of vertices. This can be explained by the roadmap not fully expanding to the small areas of the map that are also visible in 2d. But since we are sampling these for comparability with a fixed number of vertices, these vertices are needed to cover the wider areas of the map and can't penetrate into smaller areas.

C. Query Efficiency (Online Runtime)

To evaluate the query efficiency of the roadmap we use the metric of visited vertices during the A* path planning algorithm when planning a path between two random points in C_{free} . This metric serves as a comparable measurement of efficiency during the query phase, as the path planning process is quicker when it expands fewer vertices.

In Fig. 7, we show the average number of visited vertices in A* path planning for different roadmap types on different maps. In comparison to the PRM algorithm, the GSRM algorithm has a similar number of visited vertices to the lowest number of visited vertices of the other algorithms. It is visible that there is a positive correlation between the number of vertices and the number of visited vertices. But the GSRM algorithm is the lowest for all maps and across different numbers of vertices.

D. Roadmap Construction (Offline Runtime)

The runtime is an important factor for the applicability of the roadmap generation algorithm. We measure the runtime on an Intel Core i7-11850H CPU with 32 GB of RAM. The GSRM algorithm is expensive to compute, but its runtime

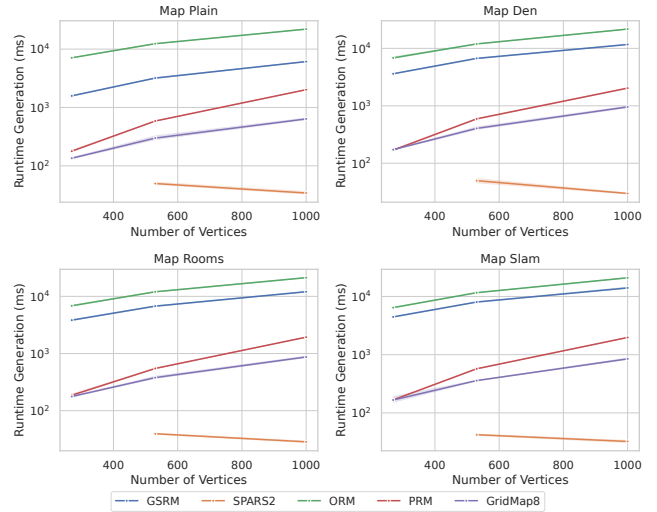


Fig. 8. Runtime of the different algorithms for the roadmap generation. The shaded areas show the standard deviation. GSRM has the second-lowest runtime.

never exceeds 10 seconds on any of the maps up to 2000 vertices.

Fig. 8 shows the runtime of the different algorithms for the roadmap generation. Especially, the SPARS2 algorithm has a very small runtime. The only algorithm that is slower than GSRM is the ORM algorithm.

VI. CONCLUSION

We present GSRM, a new algorithm for roadmap generation for path planning of mobile robots. Algorithmically, we combine reaction-diffusion systems and triangulation. Empirically, GSRM exhibits a good tradeoff between path-length, query-efficiency, and computational effort compared to the state-of-the-art. In future work, we plan to extend the algorithm to 3D and to evaluate it in multi-agent scenarios with distance constraints.

REFERENCES

- [1] W. Chen and M. J. Ward, "The Stability and Dynamics of Localized Spot Patterns in the Two-Dimensional Gray-Scott Model," *SIAM Journal on Applied Dynamical Systems*, vol. 10, no. 2, pp. 582–666, 2011.
- [2] B. N. Delaunay, "Sur la Sphère Vide," *Bulletin of Academy of Sciences of the USSR*, vol. 7, no. 6, 1934.
- [3] L. Kavraki, P. Svestka, J.-C. Latombe, and M. Overmars, "Probabilistic roadmaps for path planning in high-dimensional configuration spaces," *IEEE Transactions on Robotics and Automation*, vol. 12, no. 4, pp. 566–580, 1996.
- [4] P. Hart, N. Nilsson, and B. Raphael, "A Formal Basis for the Heuristic Determination of Minimum Cost Paths," *IEEE Transactions on Systems Science and Cybernetics*, vol. 4, no. 2, pp. 100–107, 1968.
- [5] R. Geraerts and M. H. Overmars, "A Comparative Study of Probabilistic Roadmap Planners," *Springer Tracts in Advanced Robotics*, pp. 43–57, 2004.
- [6] S. Karaman and E. Frazzoli, "Sampling-based Algorithms for Optimal Motion Planning," *International Journal of Robotics Research*, vol. 30, no. 7, 2011.
- [7] A. Dobson, A. Krontiris, and K. E. Bekris, "Sparse roadmap spanners," *Springer Tracts in Advanced Robotics*, vol. 86, pp. 279–296, 2013.

- [8] A. Dobson and K. E. Bekris, "Improving sparse roadmap spanners," in *2013 IEEE International Conference on Robotics and Automation*, 2013, pp. 4106–4111.
- [9] B. Ichter, E. Schmerling, T.-W. E. Lee, and A. Faust, "Learned Critical Probabilistic Roadmaps for Robotic Motion Planning," in *2020 IEEE International Conference on Robotics and Automation (ICRA)*, 2020, pp. 9535–9541.
- [10] S. M. Lavalle, "Rapidly-Exploring Random Trees: A New Tool for Path Planning," *The annual research report*, 1998.
- [11] H. Choset, S. Walker, K. Eiamsa-Ard, and J. Burdick, "Sensor-Based Exploration: Incremental Construction of the Hierarchical Generalized Voronoi Graph," *The International Journal of Robotics Research*, vol. 19, no. 2, pp. 126–148, 2000.
- [12] M. Kallmann, "Dynamic and Robust Local Clearance Triangulations," *ACM Transactions on Graphics*, vol. 33, no. 5, pp. 1–17, 2014.
- [13] E. G. Tsardoulis, A. T. Serafi, M. N. Panourgia, A. Papazoglou, and L. Petrou, "Construction of Minimized Topological Graphs on Occupancy Grid Maps Based on GVD and Sensor Coverage Information," *Journal of Intelligent & Robotic Systems*, vol. 75, no. 3-4, pp. 457–474, 2014.
- [14] J. Modayil, P. Beeson, and B. Kuipers, "Using the topological skeleton for scalable global metrical map-building," in *2004 IEEE/RSJ International Conference on Intelligent Robots and Systems (IROS)*, vol. 2. IEEE, 2004, pp. 1530–1536.
- [15] M. Rezaeejad, B. Samari, I. Rekleitis, K. Siddiqi, and G. Dudek, "Robust environment mapping using flux skeletons," in *2015 IEEE/RSJ International Conference on Intelligent Robots and Systems (IROS)*. IEEE, 2015, pp. 5700–5705.
- [16] T. Musil, M. Petrik, and M. Saska, "SphereMap: Dynamic Multi-Layer Graph Structure for Rapid Safety-Aware UAV Planning," *IEEE Robotics and Automation Letters*, vol. 7, no. 4, pp. 11 007–11 014, 2022.
- [17] T. Noël, S. Kabbour, A. Lehuger, E. Marchand, and F. Chaumette, "Disk-Graph Probabilistic Roadmap: Biased Distance Sampling for Path Planning in a Partially Unknown Environment," in *2022 IEEE/RSJ International Conference on Intelligent Robots and Systems (IROS)*, 2022, pp. 5707–5714.
- [18] C. Henkel and M. Toussaint, "Optimized Directed Roadmap Graph for Multi-Agent Path Finding Using Stochastic Gradient Descent," in *The 35th ACM/SIGAPP Symposium on Applied Computing (SAC '20)*, 2020.
- [19] F. Pratissoli, R. Brugioni, N. Battilani, and L. Sabattini, "Hierarchical Traffic Management of Multi-AGV Systems With Deadlock Prevention Applied to Industrial Environments," *IEEE Transactions on Automation Science and Engineering*, pp. 1–15, 2023.
- [20] M. Debord, W. Hönig, and N. Ayanian, "Trajectory Planning for Heterogeneous Robot Teams," in *2018 IEEE/RSJ International Conference on Intelligent Robots and Systems (IROS)*, 2018, pp. 7924–7931.
- [21] A. M. Turing, "The Chemical Basis of Morphogenesis," *Philosophical Transactions of the Royal Society of London B*, 1952.
- [22] P. Gray and S. K. Scott, "Autocatalytic reactions in the isothermal, continuous stirred tank reactor: Oscillations and instabilities in the system $A + 2B \rightarrow 3B$; $B \rightarrow C$," *Chemical Engineering Science*, vol. 39, no. 6, pp. 1087–1097, 1984.
- [23] A. Adamatzky, B. de Lacy Costello, C. Melhuish, and N. Ratcliffe, "Experimental Reaction-Diffusion Chemical Processors for Robot Path Planning," *Journal of Intelligent and Robotic Systems*, vol. 37, no. 3, pp. 233–249, 2003.
- [24] A. Adamatzky, P. Arena, A. Basile, R. Carmona-Galán, B. D. L. Costello, L. Fortuna, M. Frasca, and A. Rodríguez-Vázquez, "Reaction-Diffusion Navigation Robot Control: From Chemical to VLSI Analogic Processors," *IEEE Transactions on Circuits and Systems I: Regular Papers*, vol. 51, no. 5, 2004.
- [25] E. Aidman, V. Ivancevic, and A. Jennings, "A coupled reaction-diffusion field model for perception-action cycle with applications to robot navigation," *International Journal of Intelligent Defence Support Systems*, vol. 1, 2008.
- [26] A. Vázquez-Otero, J. Faigl, and A. P. Munuzuri, "Path planning based on reaction-diffusion process," in *2012 IEEE/RSJ International Conference on Intelligent Robots and Systems*. Vilamoura-Algarve, Portugal: IEEE, 2012, pp. 896–901.
- [27] K. Dale and P. Husbands, "The evolution of reaction-diffusion controllers for minimally cognitive agents," *Artificial life*, vol. 16, no. 1, pp. 1–19, 2010.
- [28] A. Vázquez-Otero, J. Faigl, N. Duro, and R. Dormido, "Reaction-Diffusion based Computational Model for Autonomous Mobile Robot Exploration of Unknown Environments," *Int. J. Unconv. Comput.*, 2014.
- [29] A. Vázquez-Otero, J. Faigl, R. Dormido, and N. Duro, "Reaction Diffusion Voronoi Diagrams: From Sensors Data to Computing," *Sensors*, vol. 15, no. 6, pp. 12 736–12 764, 2015.
- [30] J. E. Pearson, "Complex patterns in a simple system," *Science*, vol. 261, no. 5118, pp. 189–192, 1993.
- [31] S. Suzuki and K. be, "Topological structural analysis of digitized binary images by border following," *Computer Vision, Graphics, and Image Processing*, vol. 30, no. 1, pp. 32–46, 1985.
- [32] R. Stern, N. Sturtevant, A. Felner, S. Koenig, H. Ma, T. Walker, J. Li, D. Atzmon, L. Cohen, T. K. S. Kumar, E. Boyarski, and R. Bartak, "Multi-Agent Pathfinding: Definitions, Variants, and Benchmarks," in *Proceedings of the International Symposium on Combinatorial Search*, 2019.